Journal of Applied Electrochemistry **29**: 961–970, 1999.

Electrolytic oxidation of trichloroethylene using a ceramic anode

G. CHEN[1], E.A. BETTERTON[2] and R.G. ARNOLD[1]*
[1]*Department of Chemical and Environmental Engineering and*
[2]*Department of Atmospheric Sciences, University of Arizona, Tucson, AZ 85721, USA*
*(*author for correspondence, e-mail: arnold@engr.arizona.edu; fax: +1 520 6216048)*

Received 8 August 1998; accepted in revised form 18 December 1998

Key words: ceramic electrode, Ebonex®, electrochemical oxidation, spin-trap technique, trichloroethylene

Abstract

Trichloroethylene (TCE) was transformed to CO_2, CO, Cl^- and ClO_3^- at the anode of a two-chambered electrolytic cell. The working electrode was constructed from Ebonex®, an electrically conductive ceramic (Ti_4O_7). Under our experimental conditions (anode potential E_a = 2.5 to 4.3 V vs SSCE), the disappearance of TCE was first order in TCE concentration. The transformation rate was independent of pH in the range $1.6 < pH < 11$. TCE oxidation occurred only on the anodic surface and was limited by mass transport at high potentials ($E_a > 4.0$ V). The maximum (transport-limited), surface-area-normalized rate constant was about 0.002 43 cm s^{-1}. Carbon-containing products included CO_2 primarily with traces of CO. At neutral and alkaline pHs, the only chlorine-containing products were Cl^- and ClO_3^-. Hydroxyl radicals were detected in the anodic compartment using a spin trap (4-POBN). A kinetic model was successfully correlated with experimental results.

1. Introduction

Trichloroethylene (TCE) has been used widely as a degreasing agent, dry cleaning solvent and chemical extraction agent. Inappropriate disposal methods have produced widespread groundwater contamination [1]. The earliest reported discovery of TCE in groundwater was in 1979 in the vicinity of Sacramento, California [2]. Also in the late 1970s, it was determined that TCE is both a probable human carcinogen and potent toxicant [3, 4]. The US Environmental Protection Agency subsequently established the maximum contaminant level for TCE in potable water at 5 μg dm^{-3} [5, 6].

Known methods for the destruction of TCE in water include oxidative and reductive biochemical degradation [7–14], photochemical transformation [15, 16], high-energy electron beam irradiation [17, 18] and chemical oxidation [19, 20], sometimes in the presence of a transition metal catalyst or high temperature and pressure [21]. Although electroreduction of TCE has received some attention [22, 23], we could find no reports of its direct electrolytic oxidation.

Hydroxyl radicals ($OH^{\cdot}$) can be formed from the electrolytic oxidation of H_2O/OH^- [24]. They are powerful, nonspecific oxidants that react at significant rates with TCE and a variety of other organic contaminations [19, 25, 26] (Table 1). Consequently, $OH^{\cdot}$ generation may play a role in TCE electrolysis. Hydroxyl radical activity can be observed indirectly using spin traps such as α-(4-pyridyl-1-oxide) *N-tert*-butylnitrone (4-POBN) [27]. The radical adds to the unsaturated spin trap to form a new radical adduct of longer lifetime,

(1)

That can be detected using electron spin resonance (ESR) [28, 29].

Graphite, noble metals, PbO_2, Ti/SnO_2, and Ebonex® ceramic are commonly used anode materials. For this work, Ebonex® was selected as the anode material as a consequence of its electrical conductivity (6.3×10^{-4} Ω cm, similar to that of graphite [30]) and chemical stability. Ebonex® is a nonstoichiometric titanium oxide comprised of Magneli phase titanium oxides Ti_4O_7 and Ti_5O_9 [31–33]. It is made by heating TiO_2 to 1273 K in the

Table 1. Rate constants for reaction of $OH^{\cdot}$ with compounds of environmental significance

Compound	Rate constant /dm^3 mol^{-1} s^{-1}	Compound	Rate constant /dm^3 mol^{-1} s^{-1}
Phenol [25]	1.3×10^{10}	pentachlorophenol [25]	4×10^9
Toluene [25]	3×19^9	general pesticides [26]	$5 \times 10^7 \sim 1 \times 10^{10}$
m-Xylene [25]	7.5×10^9	trichloroethylene [25]	4.2×10^9
o-Xylene [25]	6.7×10^9	tetrachloroethylene [19]	3×10^9
p-Xylene [25]	7.0×10^9	1,1-dichloroethylene [19]	7×10^9
Benzene [25]	7.8×10^9	1,1-dichloroethane [19]	1.2×10^9
2-Chlorophenol [25]	1.2×10^{10}	1,1-dichloro-1-propane [19]	4×10^9
Naphthalene [25]	9×10^9	chloropentane [19]	3×10^9

presence of H_2(g). The product is stable in aqueous media throughout the practical pH range, although anodic oxidation in 1 M sulfuric acid results in partial oxidation of Ti_4O_7 to TiO_2, and surface passivation under extreme conditions may be an issue [34].

Here we describe work designed to establish the stoichiometry and kinetics of electrolytic TCE oxidation using an Ebonex® ceramic anode. The dependence of reaction rate on the fixed anode potential and bulk solution pH was investigated. Data were used to propose a mechanism and estimate kinetic parameters for TCE electrolysis. Product stoichiometry and process efficiency were established as a function of electrode potential and bulk solution pH.

2. Methods and materials

2.1. *General*

Experiments were conducted in a two-chamber, three-electrode glass reactor in which the anode and cathode compartments were separated by a 15 cm^2 Nafion® cation-exchange membrane (Fig. 1). The 320 cm^3 anode compartment contained 200 cm^3 of the electrolyte solution and a head space of 120 cm^3. The anode consisted of an 8.5 cm × 2 cm Ebonex® (Electrosynthesis, Inc., NY) ceramic sheet with a thickness of 0.2 cm. The cathode compartment volume was 100 cm^3. The cathode was a 28 cm^2 graphite rod (Alfa Aesar, MA), while a saturated silver–silver chloride electrode (SSCE; Accumet) served as reference. The chamber containing the reference electrode was separated from the anode compartment by a glass frit. Hereinafter, all potentials are reported against the SSCE.

The anode potential (E_a) was fixed (±0.01 V) relative to the reference using a potentiostat (Amel 410, Electrosynthesis, Inc., NY). The electrolytic current was ≤1.0 A and the maximum difference between anode and cathode potentials was 25 V. The pH of the anodic compartment was maintained (±0.1 pH units) via continuous addition of 0.1 M NaOH using a pH-stat Brinkmann Metrohm (691 pH meter, 614 Impulsomat and 665 Dosimat). Contents of the anode compartment (0.05 M KNO_3 electrolyte in MilliQ water, TCE etc.) were mixed continuously using a Teflon-coated, one-inch magnetic stirring bar (600 rpm).

Trichloroethylene (Aldrich, WI) was added to the anode compartment as a liquid. After allowing two hours for equilibration of gas- and liquid-phase concentrations, experiments were initiated by setting the desired anode potential at 2.5 to 4.3 V (fixed throughout single experiment). During the 3 to 7 h experiments, 20 mm^3 liquid samples were withdrawn periodically for measurement of TCE. Gas phase samples (50 mm^3 or 100 mm^3) were analysed for O_2, CO_2, CO and TCE. Additional measurements included liquid-phase inorganic carbon; Cl^- and chlorine oxyanions ClO_3^-, ClO_2^-

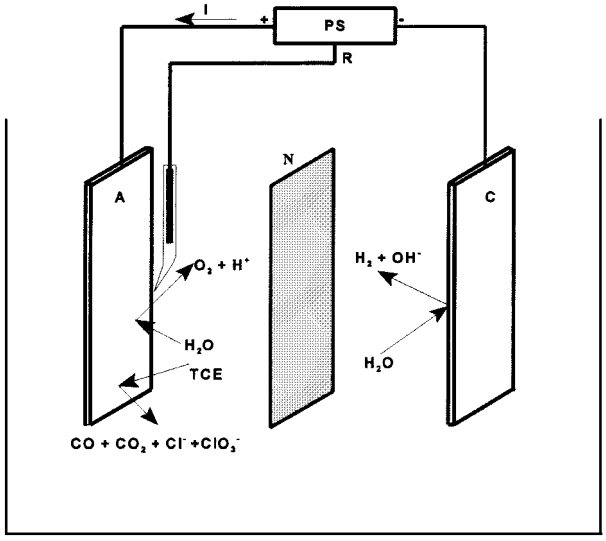

Fig. 1. Schematic representation of the electrolytic reactor including primary (expected) reactions at the anode and cathode. Key: (A) Ebonex® ceramic electrode (anode); (C) graphite cathode; (N) Nafion®, cation-exchange membrane; (PS) potentiostat; (R) saturated silver/silver chloride (reference) electrode.

and ClO^-. Liquid-phase inorganic carbon was measured by acidifying liquid samples and measuring released CO_2 gas. Chlorine gas and ClO_2 are unstable in water at pH $\geqslant$ 7.0, the pH region that was used to establish reaction stoichiometries. Independent variables other than reaction time included the fixed anodic voltage and the bulk liquid-phase pH. All experiments were conducted at room temperature (i.e., about 296–298 K).

2.2. *Analytical*

20 mm^3 liquid samples were extracted in 1 cm^3 of pentane prior to GC analysis (Hewlett-Packard 5890A; electron capture detector; DB-624 column; oven temperature 313 K, injector temperature 423 K, detector temperature 523 K; He carrier gas; flowrate 0.117 $cm^3\ s^{-1}$). Gas phase TCE was analysed using a Hewlett-Packard 5790 gas chromatography with flame ionization detector. All other operating conditions were the same as described previously. Gas phase O_2, CO_2 and CO were analysed using the HP 5790 with a Carboxen 1000 column and thermal conductivity detector (oven temperature 423 K, injector temperature 423 K, detector temperature 473 K, He carrier gas at 0.33 $cm^3\ s^{-1}$). When O_2 measurements were planned, the reactor headspace was filled with helium prior to the start of the experiment.

Inorganic ions (Cl^-, ClO^-, ClO_2^-, ClO_3^-) were analysed by ion chromatography (IC) using a Dionex Qic Analyzer (Ion-Pac AG4A guard column, HPIC-AS4A analytical column, ASRS-1 self-regenerating anion suppressor). The eluent consisted of 0.85 mM sodium bicarbonate ($NaHCO_3$)/0.9 mM sodium carbonate (Na_2CO_3) (flowrate 0.033 $cm^3\ s^{-1}$). Sample injections (25 mm^3 sample loop) were made through prerinsed 0.45 μm PTFE membrane filters (Gelman).

4-POBN was used as a spin trap to detect hydroxyl radicals produced at the reaction anode. 4-POBN (100 mM) in aqueous sodium and potassium phosphate buffer solution (VWR, PA) (pH 6–7) was used as electrolyte solution. A positive control was developed by adding H_2O_2 (100 mM) and $FeSO_4$ (100 mM) with 4-POBN to the same buffered electrolyte solution. This mixture is known to yield hydroxyl radicals via the Fenton mechanism [35]. The resulting ESR spectrum provided a signature for the 4-POBN radical adduct. A negative control was provided by adding $FeSO_4$ (100 mM) and 4-POBN (100 mM) to the same buffered electrolyte solution. To detect TCE radicals discharged at the anode surface, TCE (10 mM) was injected into the anode compartment. Samples (20 nm^3) were withdrawn from the positive and negative controls and the electrolytic reactor (anodic compartment only) for ESR analysis using a Bruker ESP 300 E spectrometer. Analyses were initiated within 10 s of sample withdrawal. The magnetic field was set at 3432.00 G; microwave frequency 9.65 GHz; modulation amplitude 3.199 G; time constant 81.92 ms; sweep time 5.5 min.

3. Mechanism and kinetic model

The mechanism that is tentatively proposed for the electrolytic oxidation of TCE consists of the following steps. TCE diffuses to the electrode surface where it undergoes a single electron oxidation, thereby contributing to the anodic current and forming a short-lived cation radical. Radical formation is assumed to be the slowest chemical transformation step on the TCE reaction pathway. Subsequent conversions involve reaction of TCE radical and/or other reaction intermediates with hydroxyl radicals. Hydroxyl radicals produced at the anode surface via oxidation of H_2O or OH^- are consumed locally in the generation of molecular oxygen or participate in the conversion of TCE and/or reaction intermediates via hydrogen abstraction or chlorine substitution. These steps are assumed to be relatively fast. Stable reaction products include CO_2, CO, Cl^- and chloroxyanions. Justification for individual steps is provided subsequently based on experimental observations.

A rate expression for TCE conversion was developed based on conservation of mass in the anodic compartment. Selecting the control volume to include both the gas and liquid phases yields

$$R_m = 10^{-3}\left[V_\ell \frac{dC_\ell}{dt} + V_g \frac{dC_g}{dt}\right] \tag{2}$$

in which R_m is the rate of TCE conversion (mol s^{-1}), V_ℓ and V_g are the liquid and gas phase volumes of the anodic compartment (cm^3) and C_ℓ and C_g are the liquid and gas phase concentrations of TCE (M).

Because TCE is converted or lost only at the anode, the rate of diffusion for TCE to the anode surface is given by

$$R_m = 10^{-3} A k_m (C_\ell - C_i) \tag{3}$$

where C_i is the TCE concentration on the anode surface; k_m is a mass transport coefficient (bulk liquid-to-electrode surface; cm s^{-1}); A is the electrode surface area (cm^2). The rate of the controlling reaction step is represented using the Butler–Volmer equation:

$$R_m = 10^{-3} A k_a C_i \exp\left(\frac{n_0 \alpha_a F E_a}{RT}\right) \tag{4}$$

where n_0 is the number of electrons transferred in the rate-limiting electrode reaction (hereinafter assumed to be 1); α_a is the anode transfer coefficient (the efficiency with which electrode potential is used to overcome the activation energy barrier to electron transfer); E_a is the anode potential (V); F (96 500 C mol^{-1}) is the Faraday constant; R (8.314 J mol^{-1} K^{-1}) is the gas constant; T (K) is the absolute temperature; k_a (cm s^{-1}) is a rate constant for electron transfer (TCE to electrode) that contains both material- and reactor-dependent parameters such as the open-circuit potential for the reaction of interest. Under quasi-steady conditions [36, 37], from Equations 3 and 4, the rate of transformation related to the liquid-phase TCE concentration can be derived as

$$R_m = 10^{-3} A C_\ell \left[\frac{1}{k_m} + \frac{1}{k_a}\exp\left(-\frac{\alpha_a F E_a}{RT}\right)\right]^{-1} \quad (5)$$

Integrating Equation 5 over time yields

$$m_0 - m = 10^{-3} A \int_0^t C_\ell \, dt \left[\frac{1}{k_m} + \frac{1}{k_a}\exp\left(-\frac{\alpha_a F E_a}{RT}\right)\right]^{-1} \quad (6)$$

where m is the mass of TCE in the reactor at time t and m_0 is the mass initially present (mol). C_ℓ and C_g were measured over the course of each experiment to support calculation of $m_0 - m$ and $\int C_\ell \, dt$. Thus, the area-specific rate of TCE conversion is predicted to be first order in C_ℓ with a rate constant that is defined by

$$k = \left[\frac{1}{k_m} + \frac{1}{k_a}\exp\left(-\frac{\alpha_a F E_a}{RT}\right)\right]^{-1} \quad (7)$$

To analyse data from a single experiment, $m_0 - m$ was plotted against $A \int C_\ell \, dt$. The slope of this curve provided a voltage-dependent estimate for k. The procedure was repeated for a variety of fixed E_a values, and the resultant relationship was used to estimate α_a, k_m and k_a for TCE oxidation at Ebonex®. Because the reactive electrode area could not be determined with certainty, the geometric electrode area was used in the calculation. To the extent that this procedure underestimates the effective electrode area, k and therefore k_m and k_a are overestimated.

4. Results and discussion

4.1. *Detection of OH radicals*

As expected, an aqueous mixture of 4-POBN and $FeSO_4$ produced no detectable radicals (Fig. 2(a)). When H_2O_2 was also added to generate radicals via Fenton's mechanism [35] (positive control), the ESR spectrum of the 4-POBN-OH adduct was obtained (Fig. 2(b)). The similarity of the ESR spectrum derived from the oxidation of water at Ebonex® (Fig. 2(c)) strongly

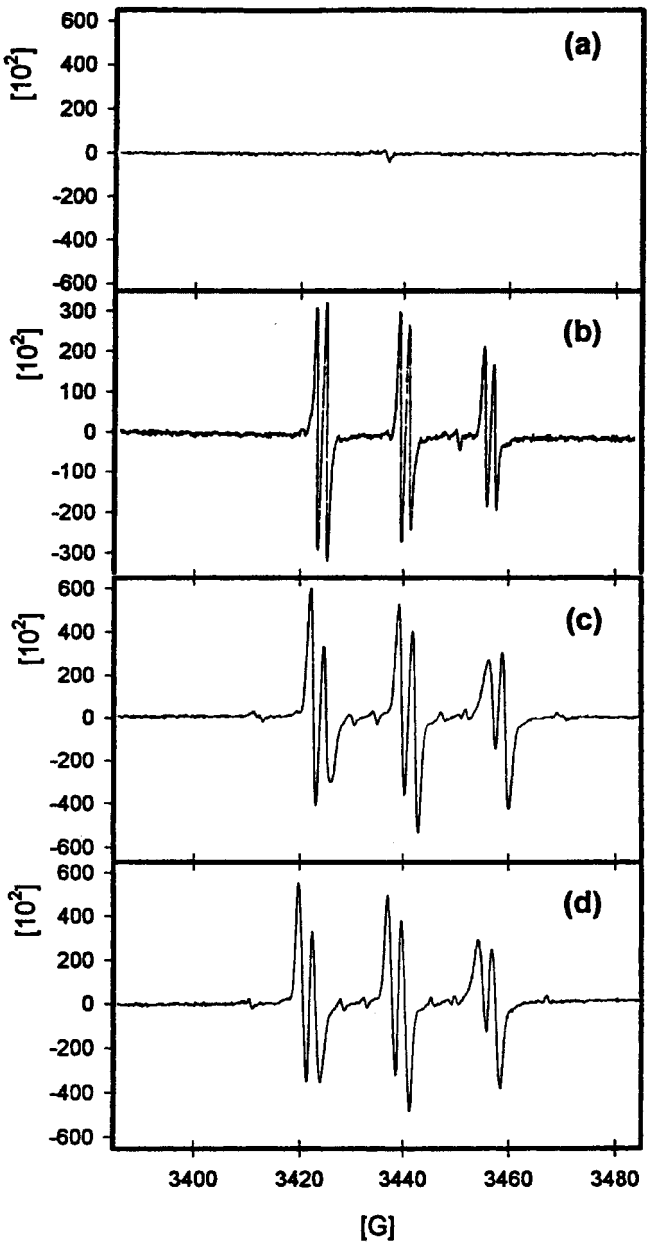

Fig. 2. ESR spectra for radical adducts obtained using the following aqueous solutions/experimental conditions: (a) 100 mM 4-POBN; 100 mM $FeSO_4$ (negative control); (b) 100 mM 4-POBN; 100 mM $FeSO_4$; 100 mM H_2O_2 (positive control); (c) anode electrolysis; 50 min at 120 mA with an Ebonex® electrode; 100 mM 4-POBN; (d) anode electrolysis; 50 min at 120 mA with an Ebonex® electrode; 100 mM 4-POBN plus 10 mM TCE. Note that experiments (c) and (d) differed only via the addition of TCE to the aqueous 4-POBN solution.

suggests that hydroxyl radicals are produced under the conditions of the experiment. Addition of TCE did not alter the spectrum (Fig. 2(d)) suggesting (i) that at the concentrations used TCE was not an appreciable sink for hydroxyl radicals and (ii) that, if formed, TCE radical did not react with 4-POBN to produce a stable adduct.

4.2. *Variation of anode potential*

Eleven experiments were carried out at anode potentials ranging from 2.5 to 4.3 V, pH 7.0 and an initial TCE concentration near 1.0 mM. Time-dependent TCE data are summarized in Figure 3. The vertical axis is the (normalized) time-dependent mass of TCE in the reactor. Although resistance to mass transfer across the air/water interface may contribute to the overall resistance to transformation in the reactor, here no assumption is made regarding the attainment of Henry's law equilibrium. Nor is one necessary since both gas- and liquid-phase concentrations of TCE were routinely measured. That is, the mass balance that produced Equations (2–7) was based on a control volume comprised of the entire anodic compartment. Mass transfer across the air/liquid interface does not show up explicitly although interphase transport resistance may be a strong determinant of R_m. Despite this limitation, the selection of control volume and resultant analysis (parameter estimation) are appropriate for situations in which the kinetics of mass transport across the gas/liquid interface is not an issue.

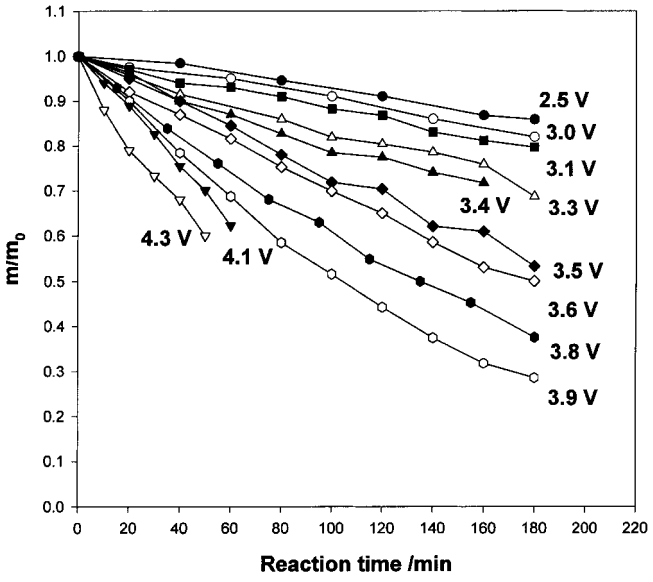

Fig. 3. Disappearance of TCE from the anode compartment of the electrolytic cell (Figure 1) using an Ebonex® ceramic electrode; pH 7.0; anode potential as indicated. Note that m is the mass of TCE in the electrode compartment, or $V_\ell C_\ell + V_g C_g$, and m_0 is the mass of TCE in the anode compartment at the onset of the experiment.

Figure 3 data were used to relate the mass of TCE transformed to the quantity $A \int C_l \, dt$ (Fig. 4). Slopes were used to estimate k values (Equations 6 and 7) as a function of E_a (Fig. 5) and then to estimate k_a, k_m, and α_a using nonlinear regression analysis (Sigmaplot) [38]. Parameter estimates so obtained were $\alpha_a = 0.089$; $k_m = 2.43 \times 10^{-3}$ cm s^{-1}; $k_a = 6.27 \times 10^{-9}$ cm s^{-1}. Agreement between data and the fitted model was acceptable (Fig. 5). At $E_a = 3.7$ V, k was about half of its maximum value, k_m, suggesting that resistance to transformation due to mass transfer and electrode polarization were about equal at that voltage. The surface-area-normalized rate constant k, is predicted to reach k_m, its transport-limited value ($\sim$0.00243 cm s^{-1}) at $E_a > 4.5$ V. It proved difficult to achieve such rates experimentally due to rapid O_2 formation at the higher potentials tested. At $E_a = 4.5$ V, the total anodic current had not yet peaked (data not shown), suggesting that TCE oxidation occurs at the anode surface, that is, that reactive intermediates such as OH$^\cdot$ generated at the anode were not responsible for TCE oxidation in bulk solution.

4.3. *pH dependence*

The rate of production of OH$^\cdot$ should be pH dependent at pH > 7.0 due to oxidation of OH$^-$ [24]. A degree of pH dependence would be expected, at least in basic solution, if reaction with OH$^\cdot$ controls the overall rate of TCE disappearance. Five experiments were carried out at $E_a = 3.5$ V and pH values ranging from 1.6 to 11.0. Results (Figure 6) indicate that the rate of TCE disappearance was independent of solution pH, suggesting that assumptions regarding the origin of overall rate limitation are justified. That is, the rate-controlling step in the proposed mechanism for TCE oxidation apparently does not involve reaction with OH$^\cdot$.

4.4. *TCE concentration effects*

Three additional experiments were conducted at an initial liquid phase TCE concentration of approximately 1.0 μM (pH 7.0; E_a 3.1, 3.5 and 3.8 V) to see if kinetic relationships developed at millimolar concentrations extended into the micromolar concentration range. Conditional first-order rate constants (k values: 4.17×10^{-4}, 7.3×10^{-4} and 1.45×10^{-3} cm s^{-1}) were similar to values reported in Figure 5. The mechanism of TCE oxidation, including the source of rate limitation, was apparently unaltered by a three order-of-magnitude reduction in TCE concentration.

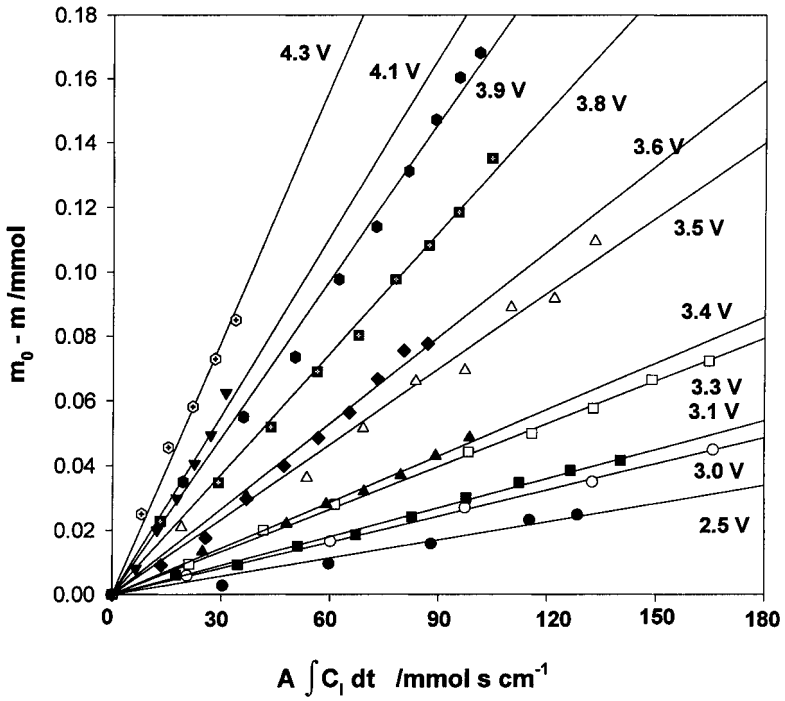

Fig. 4. Mass of TCE transformed (from data in Fig. 3) as a function of $A \int C_\ell \, dt$. Reactor conditions were as indicated in Figure 3 and the text. Regression lines were constrained to pass through the origin. Goodness of fit supports the kinetic model used here (Equation 5). Notice that slopes are estimates of voltage-dependent k values (Equation 7).

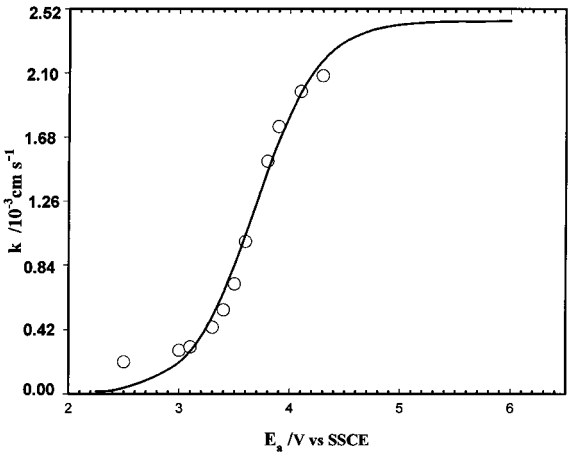

Fig. 5. Voltage-dependent, surface area-normalized, first order (in TCE concentration) rate constants (k) for TCE oxidation at the Ebonex® ceramic anode, pH 7.0. The solid line is the best fit to Equation 7. Fitting parameters (k_m, k_a, α_a) were obtained using a nonlinear curve-fitting algorithm (Sigmaplot).

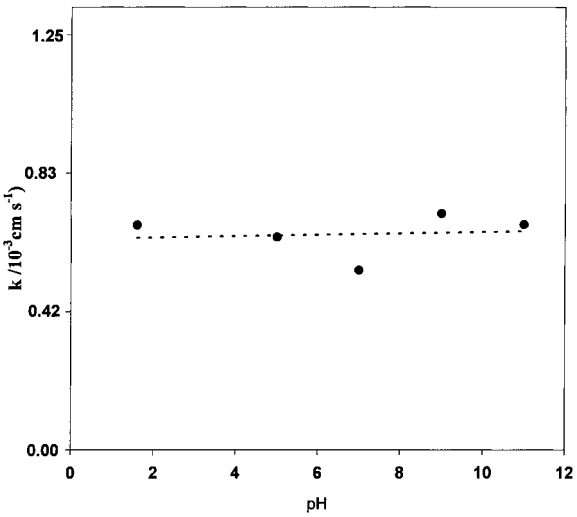

Fig. 6. Surface area-normalized rate constants for TCE oxidation at an Ebonex® ceramic anode (E_a = 3.5 V) as a function of the bulk solution pH.

4.5. *Reaction stoichiometry*

Experiments to establish a carbon balance (Fig. 7) and a chlorine balance (Fig. 8) generally indicated that all major carbon- and chlorine-containing products of TCE decomposition were accounted for analytically. CO and CO_2 were the only major carbon-containing products of TCE oxidation. At $E_a = 3.8$ V and pH 1.6 to 1.9, CO_2 accounted for about 90% of the TCE carbon transformed over the 400 min course of the experiment

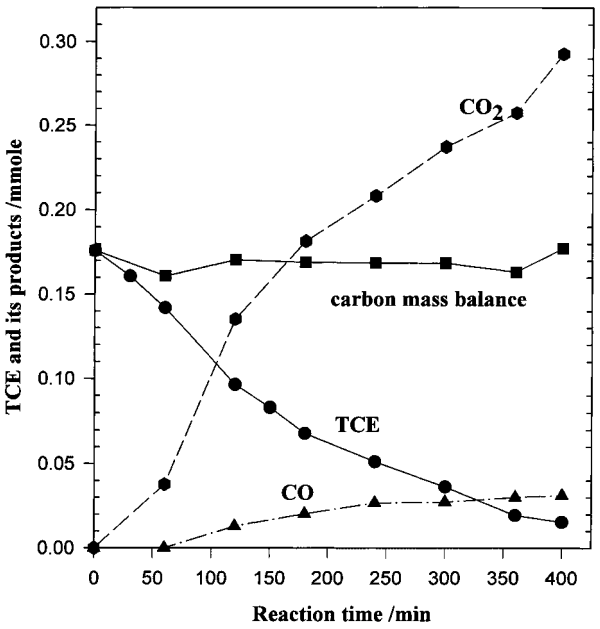

Fig. 7. TCE oxidation at an Ebonex ceramic electrode (E_a = 3.8 V). Solution pH was allowed to drift between 1.6 and 1.9 in this experiment. Notice that major carbon-containing products of TCE oxidation included only CO_2 and CO, as indicated by the mass balance on carbon. The mass balance line was calculated as TCE + (CO_2 + CO)/2 (all masses in mmol).

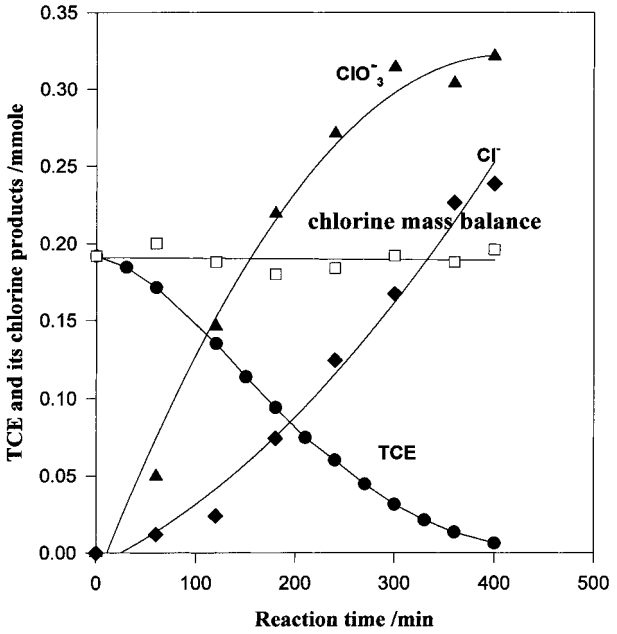

Fig. 8. TCE oxidation at an Ebonex ceramic electrode (E_a = 4.0 V; pH 7.0). Note that major chlorine-containing products of TCE oxidation included only Cl^- and ClO_3^-, as indicated by the mass balance on chlorine. The mass balance line was calculated as TCE + (Cl^- + ClO_3^-)/3 (all masses in mmol).

(Fig. 7). The remaining 10% appeared as CO. The ratio of CO_2 to CO produced proved to be approximately constant in experiments conducted from $E_a = 2.5$ to 4.0 V (Table 2). Solution pH was generally in the acid range (and uncontrolled) in these experiments to facilitate measurement of CO_2 evolution. Hence a range of pH values is reported for each experiment.

Expected chlorine-containing products were Cl^-, ClO^-, ClO_2^-, ClO_3^-, ClO_2(g) and Cl_2(g). Potential intermediates ClO_2^- and ClO^- were not observed, probably due to hydrolysis and/or reaction with $OH^{\cdot}$. At pH $\geqslant$ 7.0, Cl_2(g) and ClO_2(g) should hydrolyse at the anode surface to produce ClO^- and ClO_3^- [39], and, in fact, the only chlorine-containing species detected in the experiment conducted at pH 7.0 were Cl^- and ClO_3^- (Figure 8). All the chlorine initially present as TCE was accounted for within the limits of analytical accuracy.

4.6. *Current efficiency*

As expected, oxygen generation was observed at the reactor anode in the course of these experiments. Oxygen generation may have several deleterious effects on reactor performance. Most obvious is a loss of efficiency since power requirements and operations costs are oblivious to the nature or identity of the anodic reactions. Oxygen generation may also result in a loss of effective electrode surface area due to bubble generation/attachment. Here we defined a current efficiency in terms of the fraction of total anodic current that is accounted for via a specific reaction or set of reactions. For example, the fraction of current that results in (TCE) carbon oxidation was defined as

$$\eta_{CO+CO_2} = \frac{3Fm_{CO_2} + Fm_{CO}}{\int i_a \, dt} \tag{8}$$

Table 2. Carbon mass balance and the ratio of the carbon products for TCE anodic oxidation at different potentials. Reaction time was 180 min

E_a/V	2.5	3.0	3.5	3.8	4.0
pH	3.3 ~ 2.3	4.4 ~ 1.7	2.2 ~ 1.1	1.9 ~ 1.5	3.1 ~ 2.2
Δm_{TCE} (mmol)	0.0248	0.0474	0.110	0.135	0.168
m_{CO} (mmol)	0.0042	0.0070	0.0188	0.0187	0.0390
m_{CO_2} (mmol)	0.0425	0.0721	0.195	0.237	0.332
m_{CO_2}/m_{CO}	10.1	10.3	10.4	12.6	8.5

where m_i represents the mass of component i produced over the course of an experiment (in mol) and $\int i_a \, dt$ is the cumulative anodic charge transfer over the same period (in C). F is the Faraday constant. In this manner, the fraction of anode charge transfer for chlorine oxidation was

$$\eta_{Cl^- + ClO_3^-} = \frac{6Fm_{ClO_3^-}}{\int i_a \, dt} \tag{9}$$

(assuming that Cl^- and ClO_3^- were the sole chlorine-containing products), and, for oxygen production,

$$\eta_{O_2} = \frac{4Fm_{O_2}}{\int i_a \, dt} \tag{10}$$

Stoichiometric coefficients were based on the relative oxidation states of carbon in TCE, CO_2 and CO, and the oxidation states of chlorine in chloride ion, chlorate etc. Conditional efficiencies for CO_2 and CO production at $2.5 \text{ V} < E_a < 3.9 \text{ V}$ (Figure 9) indicate that TCE transformation efficiency was inversely related to the anode potential. The highest value observed was 32%, at $E_a = 2.5$ V. The distribution of anodic current among reaction products is also illustrated in Figure 10. Again it is evident that a smaller fraction of anodic current arises from TCE destruction at the higher voltages. The loss of efficiency is compensated for by faster reaction kinetics. The inverse relationship between voltage and current efficiency probably arises from TCE mass transport limitation at the higher voltages. However, the relatively low transfer coefficient ($\alpha_a = 0.089$) for TCE oxidation should also be noted in this context. That is, since mass transfer of H_2O should not limit the O_2 production rate, constraints on TCE transformation arising from mass transport of TCE to the electrode surface should lower $\eta_{CO_2 + CO}$ (as well as $\eta_{Cl^- + ClO_3^-}$). Furthermore, if α_a (TCE oxidation) $< \alpha_a$ (H_2O oxidation), increased anode potential and TCE conversion rate should be accompanied by lower current efficiency.

The practicality of electrolytic decomposition of halogenated aliphatics remains to be established. Use of Ebonex® as an electrode material satisfies several needs, however, owing primarily to its conductivity and resistance to corrosion. In this study, repeated use of electrodes over periods of weeks to months produced no apparent surface passivation in the aqueous potassium nitrate electrolyte and at the voltages used. All work reported was accomplished using a single anode. Electrode cleaning procedures consisted of only a rinse

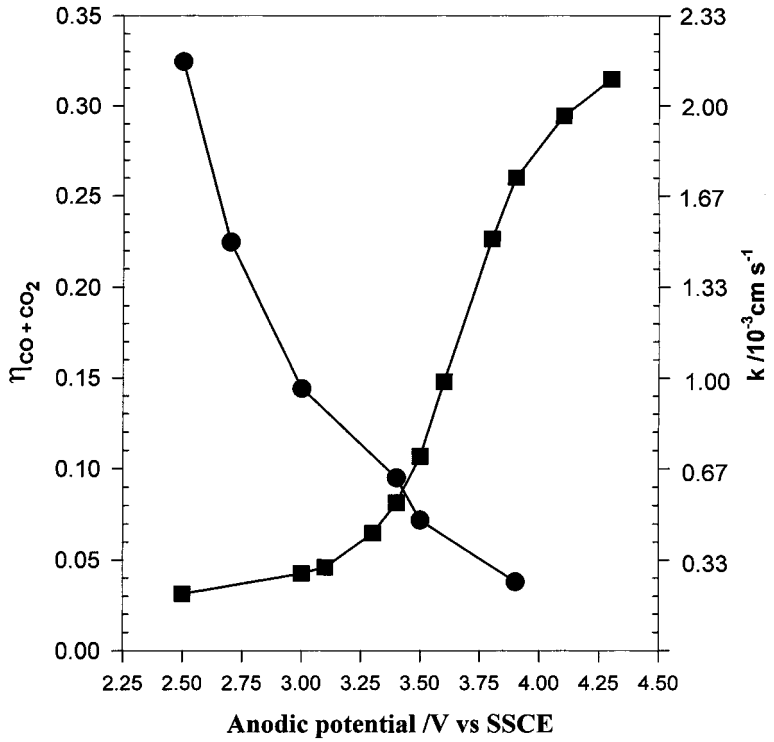

Fig. 9. Fraction of anodic current that is accounted for by the conversion of TCE to CO_2 and CO (●) and the surface area-normalized rate constant (k; ■) as functions of the fixed anode potential.

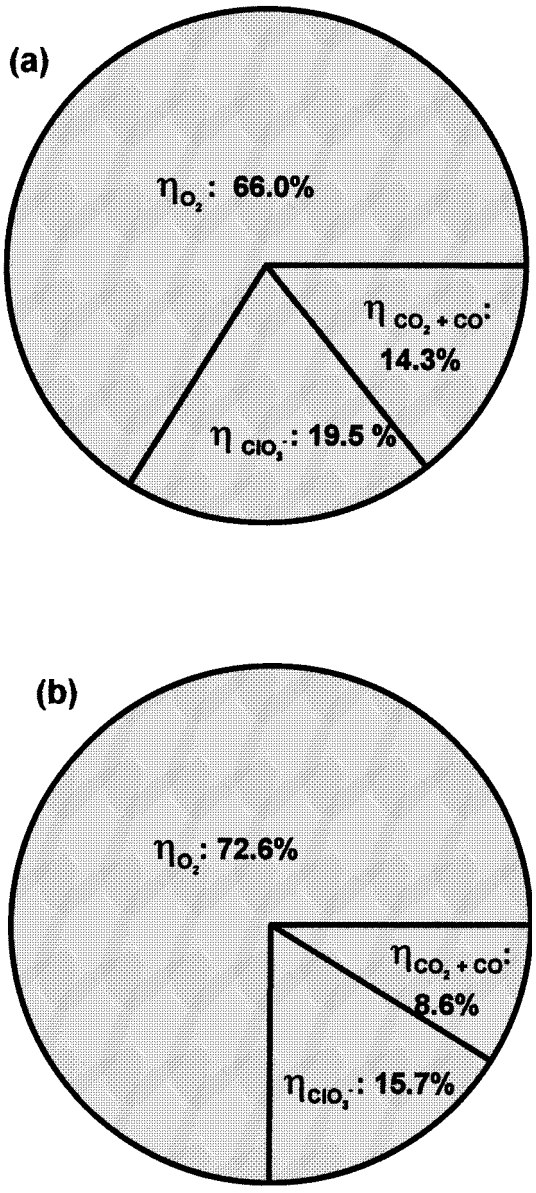

Fig. 10. Percentage of anodic current accounted for by TCE (carbon and chlorine) oxidation and O_2 production. (a) E_a = 3.0 V; (b) E_a = 3.4 V. Both experiments were conducted at pH 7.0.

in MilliQ water. Results were reproducible, as indicated by repeated, identical experiments (not shown), and the body of data generated offers the appearance of internal consistency. Additional work will be necessary to determine effects due to long-term electrode passivation, especially in an actual ground water. The effect of solution ionic strength on transformation kinetics also remains to be established. Ebonex® ceramic is available as a permeable solid that should be well suited for use as a flow-through treatment electrode with a favourable surface-to-volume ratio [40]. Additional work is necessary, however, to establish design parameters: for example, electrode thickness and flowrate, for applications such as the oxidation of halogenated ethenes.

Ebonex® enjoys large overpotentials for both oxygen and hydrogen evolution in water. Its overpotential for water oxidation is evident since, for $2H_2O \rightarrow O_2 + 4H^+ + 4e^-$, $E^\circ_w = -0.62$ V vs SSC [41], which is significantly lower than potentials employed in this study. Overpotential for hydrogen evolution may make Ebonex® a useful material for reductive transformation of TCE and related compounds, although this remains to be established.

Equation 7 provides a reasonable point from which to evaluate the feasibility of groundwater treatment via an oxidative electrolytic strategy. The fitted coefficients k_a and α_a are intrinsic to the oxidation of TCE at Ebonex®, and, although k_m is a function of reactor hydraulics, the value generated here should be a conservative estimate of what can be achieved in a flow-through electrode. From this work, $k = 1.25 \times 10^{-3}$ cm s^{-1} at $E_a = 3.7$ V. For advection-dominated plug flow through a porous Ebonex® electrode, electrode volume requirements are governed by

$$V_a = \frac{Q}{k\hat{A}\theta}\ln\left(\frac{C_0}{C_e}\right) \tag{11}$$

where V_a is the volume of the anode compartment (dm^3); Q is the flow rate of the stream to be treated (dm^3 s^{-1}); $\hat{A}$ is the area-to-volume ratio of the anode material (cm^{-1}); θ is the anode porosity; and C_0 and C_e are the influent and effluent concentrations of the target contaminant. For an electrode of specific surface area = 2000 cm^2 g^{-1}, density = 4 g cm^{-3}, $\theta = 0.8$ (representative values from the manufacturer's specifications) an order-of-magnitude oxidation in TCE could be achieved with a detention time of about 2 s. At a design flow rate of 0.17 dm^3 s^{-1}, the required anode volume would be 240 cm^3. It may be possible to improve electrode performance characteristics via the deposition of metal coatings [35] although this remains to be demonstrated for TCE transformations.

5. Conclusions

TCE was rapidly oxidized to CO and CO_2 using an Ebonex® ceramic anode. There were no other major carbon-containing products. In the neutral and alkaline pH range, the only chlorine products detected were Cl^- and ClO_3^-. TCE oxidation kinetics were limited by diffusive transport at $E_a \geqslant 4.0$ V. The maximum surface-

area-normalized rate constant was 0.002 43 cm s^{-1}. The efficiency for TCE oxidation was inversely related to the anode potential, probably because TCE transport limitations became more restrictive at higher voltages. The disappearance of TCE was first-order in TCE concentration in experiments conducted at initial concentrations from 1.0 μM to 1.0 mM. Conditional first-order rate constants obeyed the same voltage dependence in each TCE concentration range tested.

The physical and kinetic models proposed in this work were in agreement with experimental results. Electron transfer from TCE to the anode surface apparently limited the overall rate of reaction at relatively low applied potentials, and mass transport limited reaction kinetics at higher anode potentials. Anode polarization and mass transport provided equivalent resistance to reaction at $E_a \cong 3.7$ V. Hydroxyl radicals were produced at the electrode surface and probably participated in the overall transformation, although those reactions did not limit the rate of TCE disappearance under the experimental conditions. The extent to which hydroxyl radical generation is responsible for product selection or, under other experimental conditions, assists in the determination of TCE conversion rate remains to be established.

Acknowledgements

This publication was made possible by grant number P42 ES004940 from the National Institute of Environmental Health Sciences, NIH with funding provided by EPA.

References

1. P.C. Millett and J.N. Engl, *J. Water Works Assoc.* **109**(2) (1995) 140.
2. F.D. Schaumburg, *Environ. Sci. Technol.* **24**(1) (1990) 17.
3. V. Karel, *Handbook of Environmental Data on Organic Chemicals*, 2nd edn, Elsevier, New York (1983).
4. A.M. Fan, *Rev. Environ. Contam. Toxicol.* **101** (1988) 55.
5. F.W. Pontius, *J. AWWA* **2** (1990) 32.
6. Public Law 99-339. *Safe Drinking Water Act Amendments of 1986* (19 June 1986) .
7. H. Uchiyama, K. Oguri, O.Yagi and E. Kokafuta. Biotechnology Letters **14**(7) (1992) 619.
8. C.D. Little, A.V. Palumbo, S.E. Herbes, M.E. Lidstrom, R.L. Tyndall and P.J. Gilmer, *Appl. Environ. Microbiol.* **54**(4) (1988) 951.
9. M.J.K. Nelson, S.O. Montgomery, E.J. O'neill and P.H. Pritchard, *Appl. Environm. Microbiol.* **52**(2) (1986) 383.
10. B.D. Ensley, *Annu. Rev. Microbiol.* **45** (1991) 283.
11. W.W. Mohn and J.M. Tiedje, *Microbiol. Rev.* **56**(3) (1992) 482.
12. G.R. Chaudhry and S. Chapalamadugu, *Microbiol. Rev.* **55**(1) (1991) 59.
13. M.L. Hanna and R.T. Taylor, *Biotechnol. and Bioeng.* **51** (1996) 659.
14. M.W. Fitch, J. Weissman, P. Phelps, G. Georgiou and G.E. Speitel Jr, *Wat. Res.* **30**(11) (1996) 2655.
15. Y. Zhang, J.C. Crittenden, D.W. Hand and D.L. Perram, *Environ. Sci. Technol.* **28**(3) (1994) 435.
16. M.R. Prairie, T.E. Pacheco and L.R. Evans, INT. Solar Energy Conference, ASME, New York (1992).
17. W.J Cooper, D.E. Meacham, M.G. Nickelsen, K. Lin, D.B. Ford, C.N. Kurucz and T.D. Waite, *J. Air & Waste Management Ass.* **43**(10) (1993) 1358.
18. C.N. Kurucz, T.D. Waite, W.J. Cooper and M.G. Nickelson, *Phys. Chem.* **45**(5) (1995) 805.
19. S.J. Masten and J. Hoigne, *Ozone Sci. & Eng.* **14**(3) (1992) 197.
20. D.D. Gates and R.L. Siegrist, 1995. *J. Environ. Eng.* **121**(9) (1995) 639.
21. E.G. Baker and L.J. Sealock, 1988. *Catalytic Destruction of Hazardous Organics in Aqueous Solutions*. Available from the National Technical Information Service (Springfield VA 22161) as DE88-009535. Report PNL-6491-2 (April, 1988).
22. T. Nagaoka, J. Yamashita, M. Kaneda and K. Ogura, *J. Electroanal. Chem.* **335** (1992) 187.
23. T. Nagaoka, J. Yamashita, M. Takase and K. Ogura, *J. Electrochem. Soc.* **141**(6) (1994) 1522.
24. J.P. Hoare, *Encyclopedia of Electrochemistry of the Elements*, vol. 2, Marcel Dekker, New York (1974).
25. G.V. Buxton, C. Greenstock, W.P. Hellman and A.B. Ross, *J. Phys. Chem. Ref. Data* **17**(2) (1988) 513.
26. W.R. Haag and C.C.D. Yao, *Environ. Sci. Technol.* **26**(5) (1992) 1005.
27. S.G. Huling, PhD dissertation, University of Arizona, Tucson, AZ (1996).
28. K. Makino, M.M.M. Mossoba and P. Riesz, *J. Phys. Chem.* **87** (1983) 1369.
29. R.P. Mason, P.M. Hanna, M.J. Burkitt and M.B. Kadiiska, *Environ. Health Perspectives* **102** (1994) 33.
30. J.E. Graves, Doctoral thesis. Southampton University, UK (1991).
31. R.L. Clarke, Proceedings of the second international forum on *Electrolysis in the Chemical Industry*, Deerfield Beach, FA (1988).
32. P.C.S. Hayfield and R.L. Clarke, Proceedings of the electrochemical society meeting, Los Angeles, CA (1989).
33. R.L. Clarke, *Electrochemical Processing – Innovation and Progress*, Moat House International, Glasgow, UK (21–23 April) (1993).
34. J.E. Graves, D. Pletcher, R.L. Clarke and F.C. Walsh, *J. Appl. Electrochem.* **21** (1991) 848.
35. J. Walling, *Acc. Chemical Res.* **8** (1975) 125.
36. J.B. Hiskey and V.M. Sanchez, *J. Appl. Electrochem.* **20** (1990) 479.
37. Z. Liu, E.A. Betterton and R.G. Arnold, *Environmental Engineering Science* **16**(1) (1999) 1.
38. SPSS Inc., SigmaPlot$^{(R)}$ 4.0, Transforms & Regressions for Window$^{(R)}$ 95, NT and 3.1, *Reference Manual*, Chicago 8-1–8-38 (1997).
39. C.N. Sawyer and P.C. McCarty, *Chemistry for Sanitary Engineers*, 2nd edn, McGraw-Hill, New York (1967).
40. K. Rajeshwar, J.G. Ibanez and G.M. Swain, *J. Appl. Electrochem.* **24** (1994) 1077.
41. R.C. Weast and M.J. Astle, *CRC Handbook of Chemistry and Physics*, CRC press Boca Raton, FA (1980).